

An investigation of structural dimension variation in electrostatically-coupled MEMS resonator pairs using mode-localization

Graham S. Wood, *Member, IEEE*, Chun Zhao, *Member, IEEE*, Suan Hui Pu, *Member, IEEE*, Ibrahim Sari, and Michael Kraft

Abstract—If a pair of MEMS resonators are electrostatically coupled together, the vibration amplitude ratios at the resonant frequencies of the resulting coupled system are sensitive to stiffness perturbation. An imbalance between the two resonators causes the confinement of vibration energy when the system is resonating, an effect known as mode-localization. The degree of localization can be determined by extracting the amplitude ratio of the resonators through capacitive transduction. In this paper, we have fabricated MEMS devices, using a dicing-free silicon-on-insulator process, consisting of pairs of closely spaced microresonators. Each resonator consists of a clamped-clamped beam with a wider section in the middle, which is the location of the electrostatic coupling, instituted through the DC biasing of the resonators. Several devices have been fabricated, with the length of the anchor beams being varied, which influences the frequency of resonance. Stiffness imbalance between the resonators has been introduced through electrostatic spring softening, with the sensitivity of the amplitude ratio of the resonant mode shape being greater for the higher frequency, shorter anchor devices. The sensitivities of the devices in this study have been found to be 9 times greater than state-of-the-art two-degree-of-freedom mode-localized sensors.

Index Terms—MEMS, resonators, mode-localization, stiffness sensing.

I. INTRODUCTION

MICROELECTROMECHANICAL systems (MEMS) structures are utilized commonly in a wide range of applications, including pressure sensors [1], accelerometers [2]

Manuscript edited on May 26, 2016.

An earlier version of this paper was presented at the IEEE Sensors 2015 Conference and was published in its proceedings. IEEEExplore URL: [http://ieeexplore.ieee.org/xpl/articleDetails.jsp?arnumber=7370338&filter=AND\(p_Publication_Number:7350021\)](http://ieeexplore.ieee.org/xpl/articleDetails.jsp?arnumber=7370338&filter=AND(p_Publication_Number:7350021))

G. S. Wood was with the Nano Research Group, School of Electronics and Computer Science, University of Southampton, Southampton, SO17 1BJ, U.K. He is now with the Scottish Microelectronics Centre, Institute for Integrated Micro and Nano Systems, School of Engineering, University of Edinburgh, Edinburgh, EH9 3FF, U.K. (e-mail: g.s.wood@ed.ac.uk)

C. Zhao was with the Nano Research Group, School of Electronics and Computer Science, University of Southampton, Southampton, SO17 1BJ, U.K. He is now with the Nanoscience Centre, Department of Engineering, University of Cambridge, Cambridge, CB0 0FF, U.K. (e-mail: c.zhao@eng.cam.ac.uk)

I. Sari is with the Nano Research Group, School of Electronics and Computer Science, University of Southampton, Southampton, SO17 1BJ, U.K. (e-mail: is2@ecs.soton.ac.uk).

S. H. Pu is with the Nano Research Group, School of Electronics and Computer Science, University of Southampton, Southampton, SO17 1BJ, U.K. and the University of Southampton Malaysia Campus, 79200 Nusajaya, Johor, Malaysia (e-mail: shp@ecs.soton.ac.uk).

M. Kraft is with the Montefiore Institute, University of Liège, 4000 Liège, Belgium (e-mail: m.kraft@ulg.ac.be).

and energy harvesting [3]. Successful implementations of vibrating microresonators feature in timing and frequency control [4] and mixer-filters in RF transceivers [5], where reduction in size and power consumption is seen as an advantage of MEMS.

For sensing applications, the shift in resonant frequency has been used to quantify a change in the mechanical properties of a microstructure. In response to a perturbation, the stiffness of a structure can change and previously reported research has successfully measured stiffness change that has occurred in response to strain [6]–[8] and acceleration [9]. Also, resonant frequency-shift behavior has been used to characterize the residual stress of a resonator [10]. In addition, a change in the mass of a MEMS resonator has been quantified by detecting a shift in the resonant frequency [11]–[13]. A widely researched area of resonant mass sensing is the detection of various biological elements, with functionalized surfaces promoting the attachment of the target analytes [14], [15].

A more recent development in the field of microsensors exploits a phenomenon exhibited by two or more coupled microresonators, where the coupling can take the form of a mechanical or electrostatic spring. When the coupled system is resonating at one of its mode frequencies, the introduction of an irregularity between the resonators will cause mode-localization to occur. First described in 1958 [16], mode-localization is the confinement of vibration energy in an array of coupled resonators, leading to a shift in the mode shapes of the system. Mode-localized sensing has been developed to detect a change in the stiffness [17]–[19], or the mass [20], of one of either two or three electrostatically coupled microresonators. Other studies have demonstrated the mode-localization response of an array of mechanically coupled cantilevers to the attachment of a mass [21], [22]. The previously reported research has shown improvements in mass/stiffness sensitivity of up to five orders of magnitude for mode-localized sensing, when compared to resonant frequency-shift. In addition, an advantage of electrostatic coupling is that, compared to mechanical coupling, it is capable of being tuned through the adjustment of the DC bias voltages.

Building on previously reported work [23], this paper presents a study of the mode-localization behavior of pairs of electrostatically coupled resonators that have been fabricated using a dicing-free silicon-on-insulator (SOI) fabrication process. Developed for the fabrication of accelerometers and gyroscopes with large proof masses, the fabrication technique

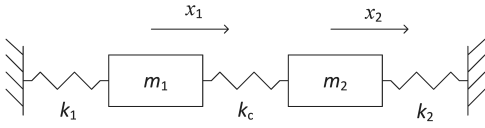


Fig. 1. Mass-spring model of a 2-DOF system consisting of two coupled resonators.

promises a high yield with no stiction during the release process [24]. The closely-spaced resonators have been designed as clamped-clamped beams with a wider section in the middle, so as to allow for potential mass loading or biological functionalization. The design differs from other work, which has characterized double-ended tuning forks [17] and wine glass ring resonators [20].

For each device, an imbalance in the relative stiffness of the two resonators has been induced electrostatically and mode-localization has been measured. The lengths of the narrow sections of the beam have been varied for different devices and the effect on the device sensitivity to a stiffness perturbation has been determined and compared to theoretical and simulated predictions.

II. THEORY

To outline the theory of mode-localization, initial theoretical analysis of a lumped-element model of a two degree-of-freedom (2-DOF) system has been performed. As shown in Fig. 1, the two resonators are each represented by a stiffness, k , and a mass, m and are coupled together with an electrostatic spring, k_c . The displacement of each resonator is given by x_1 and x_2 . Damping has been neglected in the model because all experimental measurements in this work have been performed in vacuum, which minimizes atmospheric damping.

To describe the vibration response of the system the following equations of motion are used

$$\begin{aligned} m\ddot{x}_1 + kx_1 - k_c(x_1 - x_2) &= 0 \\ m\ddot{x}_2 + kx_2 - k_c(x_2 - x_1) &= 0 \end{aligned} \quad (1)$$

where $m_1 = m_2 = m$ and $k_1 = k_2 = k$ for a balanced system. The coupling spring, k_c , is electrostatic and therefore is negative. Starting from (1), it can be shown that the system possesses two modes, with the angular frequencies represented by the square root of the following eigenvalues, λ_i ($i = 1, 2$), and the out-of-phase and in-phase mode shapes given by the eigenvectors, u_i ($i = 1, 2$)

$$\begin{aligned} \lambda_1 &= \frac{k - 2k_c}{m}, u_1 = \begin{bmatrix} x_1 \\ x_2 \end{bmatrix} = \frac{1}{\sqrt{2}} \begin{bmatrix} 1 \\ -1 \end{bmatrix} \\ \lambda_2 &= \frac{k}{m}, u_2 = \begin{bmatrix} x_1 \\ x_2 \end{bmatrix} = \frac{1}{\sqrt{2}} \begin{bmatrix} 1 \\ 1 \end{bmatrix} \end{aligned} \quad (2)$$

For the MEMS devices analyzed in this work, the closely-spaced resonators have been coupled together electrostatically by applying DC voltages to each resonator, so as to create

an electric field between them. As has been reported previously [17], for electrostatic coupling, the system has a spring constant, given by

$$k_c = \frac{(\Delta V)^2 \epsilon_0 A}{g^3} \quad (3)$$

where ΔV is the potential difference between the resonators, ϵ_0 is the permittivity of free space, g is the spacing between the two resonators and A is the cross section area of the resonators at the coupling gap.

Compared to a fixed mechanical coupling, an electrostatic coupling spring possesses the advantage of being adjustable through variation of ΔV as governed by (3). In addition, the effective stiffness of a resonator, k_1 or k_2 , can be softened by applying a DC bias to an adjacent fixed electrode. The electrostatic softening can be calculated according to (3). Altering the effective stiffness of one of the resonators using electrostatic spring softening can be used to introduce an imbalance into the 2-DOF system.

A. Mode frequencies of a perturbed system

If a stiffness perturbation Δk is added to resonator 1, the out-of-phase (ω_{op}) and in-phase (ω_{ip}) mode frequencies can be calculated from the eigenvalues, with $\lambda_{op} = \omega_{op}^2$ and $\lambda_{ip} = \omega_{ip}^2$, as follows

$$\omega_{op}^2 = \frac{1}{m} \left(k - k_c + \frac{1}{2} \left[\Delta k - \sqrt{4k_c^2 + \Delta k^2} \right] \right) \quad (4)$$

$$\omega_{ip}^2 = \frac{1}{m} \left(k - k_c + \frac{1}{2} \left[\Delta k + \sqrt{4k_c^2 + \Delta k^2} \right] \right) \quad (5)$$

From the expressions (4) and (5), it can be seen that the out-of-phase and in-phase mode frequencies never intersect and diverge if a stiffness imbalance, Δk , is introduced to the system, as explained elsewhere [25]. The relative frequency shift, $\Delta\omega_{ip}/\omega_{ip}$, that will occur in response to a relative change in the stiffness, $\Delta k/k$, of resonator 1 will be the same as the response of a 1-DOF system, which, assuming that $\Delta k \gg k_c$, is approximated by [26]

$$\frac{\Delta\omega_{ip}}{\omega_{ip}} = \frac{1}{2} \frac{\Delta k}{k} \quad (6)$$

B. Amplitude ratio of a perturbed system

The amplitude ratio shift, as a function of stiffness perturbation, at the in-phase and out-of-phase modes has been derived from (1), using a method reported previously [19]. A stiffness perturbation, Δk , due to the physical quantity to be measured, has been added to resonator 1, which is driven by a force F , so that the equations become

$$\begin{aligned} m\ddot{x}_1 + (k + \Delta k)x_1 - k_c(x_1 - x_2) &= F \\ m\ddot{x}_2 + kx_2 - k_c(x_2 - x_1) &= 0 \end{aligned} \quad (7)$$

The following expression for the amplitude ratio is obtained

$$\frac{X_1(j\omega)}{X_2(j\omega)} = \frac{-m\omega^2 + k - k_c}{-k_c} \quad (8)$$

The expressions for ω_{op}^2 and ω_{ip}^2 are obtained from (4) and (5) respectively and are substituted into (8) to give the following

$$\frac{X_1(j\omega_{op})}{X_2(j\omega_{op})} = \frac{(\Delta k - \sqrt{4k_c^2 + \Delta k^2})}{2k_c} \quad (9)$$

$$\frac{X_1(j\omega_{ip})}{X_2(j\omega_{ip})} = \frac{(\Delta k + \sqrt{4k_c^2 + \Delta k^2})}{2k_c} \quad (10)$$

The relationship between stiffness perturbation and the amplitude ratio of a 2-DOF system described by (9) and (10) has been verified by comparing to a finite-element method (FEM) simulation of a coupled MEMS system, as outlined in the next section. It is noted that the amplitude ratio response as a function of the stiffness imbalance, Δk , will be the same regardless of the initial balanced stiffness, k , of the resonators.

The sensitivity, S , of a device is defined as the change in the amplitude ratio of the resonators, $\Delta(x_1/x_2)$, as a function of the relative change in the stiffness of resonator 1, $\Delta k/k$, as shown in the expression (for $\Delta k \ll k_c$)

$$S = \frac{\Delta(x_1/x_2)}{(\Delta k/k)} = \frac{k}{2k_c} \quad (11)$$

The definition for sensitivity in (11) will be used in later sections of this paper to compare devices of different designs.

III. DESIGN OF DEVICES

A. Fabrication process

All the devices characterized in this work have been fabricated using an SOI fabrication process that has been described elsewhere [24]. Particular attention has been given to the design rules, which dictate some limits to the dimensions of the structures. Previously reported work [23] illustrates how the process has been used to create coupled resonator structures.

The process begins with a 150 mm SOI wafer with a device layer thickness of 50 μm , a buried-oxide (BOX) layer thickness of 3 μm and a handle layer thickness of 560 μm .

Plasma-enhanced chemical vapor deposition (PECVD) has been used to deposit a 1 μm layer of silicon dioxide on the front (device layer) side, and a 3 μm layer on the back (handle layer) side, of the SOI wafer. A 6 μm layer of photoresist has been spin-coated onto the front side oxide and has been patterned with photolithography. Then, inductively-coupled plasma (ICP) has been used to etch the oxide and create a mask layer for the subsequent deep reactive ion etching (DRIE) step. The back side oxide has been similarly patterned and etched.

The MEMS structures have been defined through the DRIE of trenches, with widths down to a minimum of 5 μm , in the device layer. Similarly, trenches have been etched in the handle layer, in order to define the device boundary and a block beneath the resonators. In addition to trenches, the oxide mask for the device layer has been designed to facilitate the DRIE of release holes, which allow for the release of the resonators and the device from the wafer grid, using hydrofluoric (HF) acid vapor phase etching (VPE).

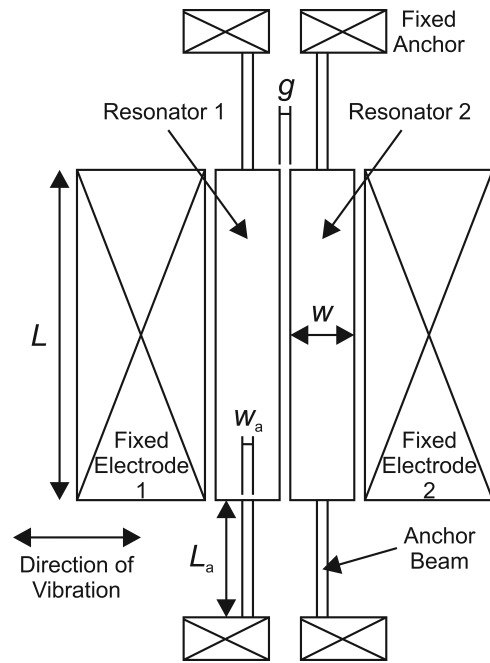


Fig. 2. Schematic of 2-DOF resonator sensing device. Not to scale.

The size and spacing of the release holes has been designed such that the resonators release first, followed by the handle block below the resonators. Finally, the HF vapor removes the oxide at the perimeter of the device, releasing the entire device from the rest of the wafer. An advantage of the fabrication process is that the individual devices are separated without the need of dicing, which can damage delicate structures.

B. Device dimensions

A schematic of the device layout is shown in Fig. 2. The device consists of a pair of resonators secured at both ends by fixed anchors, separated by a coupling gap, g . The resonators have been designed to have a wider section in the middle, with a width, w , and a length, L , to facilitate future mass loading or biological functionalization experiments. The center blocks of the resonators are secured to the fixed anchors with anchor beams of width, w_a , and length, L_a . Alongside each resonator is a fixed electrode, separated from the resonator by the same spacing as the coupling gap, g . The electrodes are used for actuation and sensing purposes, as will be explained in section III-D.

In accordance with the design rules of the fabrication process [24], any anchored area must have a minimum dimension of 300 μm to ensure that some underlying oxide remains after the device release with HF VPE. Therefore, in this work, the length, L , of the fixed electrodes alongside the resonators has been designed to be 310 μm . As a consequence of the electrode being positioned between the resonator's fixed anchors, the minimum total length ($L + L_a$) that the resonators can be is 400 μm , so as to allow for a 50 μm spacing between the electrode and each of the fixed anchor pads. Therefore, the minimum length that the anchor beams should be designed to be is 55 μm .

TABLE I
THEORETICAL MECHANICAL STIFFNESS AND MODE FREQUENCIES OF
DEVICE DESIGNS WITH COUPLING SPRING OF -15.8 N/M

Anchor beam length (μm)	k_{mech} (N/m)	f_{op} (kHz)	f_{ip} (kHz)
55	106021	1099.843	1100.007
80	34452	623.404	623.690
105	15238	420.349	420.786

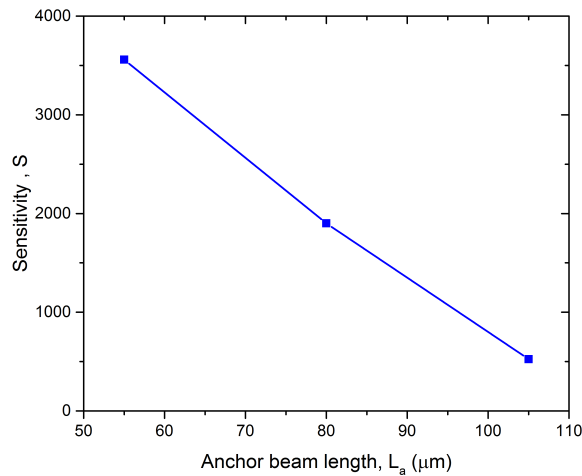


Fig. 3. Theoretical influence of anchor beam length on device sensitivity.

Given the minimum resonator dimensions allowed by the design rules, a coupled-resonator stiffness sensing device has been designed with center block dimensions of $310 \mu\text{m} \times 60 \mu\text{m}$, an anchor beam width, w_a , of $10 \mu\text{m}$ and a coupling gap, g , of $5 \mu\text{m}$. In order to determine the influence of anchor beam length on the device sensitivity, three different device designs with anchor beam lengths of $55 \mu\text{m}$, $80 \mu\text{m}$ and $105 \mu\text{m}$ have been created.

For each design, the in-plane mechanical stiffness of each of the two resonators has been calculated by treating the resonator as a pair of guided beams attached to a proof mass. The mechanical stiffness can be expressed by

$$k_{mech} = 2 \times \frac{Etw_a^3}{L_a^3} \quad (12)$$

where E is the Young's modulus of silicon in the $\langle 110 \rangle$ orientation (169 GPa) and t is the device layer thickness.

The mechanical stiffness of the three different device designs has been calculated using (12) and the influence of the anchor beam length can be seen in Tab. I, with a shorter anchor beam length resulting in a greater stiffness. Then, by calculating the response, as defined in (10), of the amplitude ratio to a stiffness perturbation, the theoretical sensitivity, S , as defined by (11), has been calculated for each of the three designs, as shown in the graph of Fig. 3. It can be seen that the sensitivity decreases with an increase in anchor beam length.

C. Electrostatic springs

DC voltages are applied to the resonators and the fixed electrodes in order to apply electrostatic spring softening to

each resonator. The effective stiffness of each of the resonators, k_1 or k_2 , is calculated by the addition of the mechanical stiffness and the electrostatic stiffness as follows

$$\begin{aligned} k_{1,2} &= k_{mech1,2} + \frac{k_{elec1,2}}{(\Delta V)^2 \epsilon_0 t L} \\ &= \frac{2Etw_a^3}{L_a^3} - \frac{k_{elec1,2}}{g^3} \end{aligned} \quad (13)$$

with the result of the negative sign of k_{elec} being that the effective stiffness of a resonator is lowered (softened) as a function of the potential difference, ΔV .

An electrostatic coupling spring, k_c , is created between the resonators by biasing them with DC voltages to create a potential difference ΔV , with the value of k_c given by (3) for $A = tL$. The devices have been designed with a coupling gap, g , of $5 \mu\text{m}$, which can be etched with DRIE reliably.

The coupling spring, k_c , and the electrostatic springs for resonator 1 and resonator 2, k_{elec1} and k_{elec2} , respectively, have been created by applying a positive DC voltage to electrode 1 and a negative DC voltage to resonator 2 and holding resonator 1 and electrode 2 at 0 V. A stiffness imbalance can be introduced to the coupled system by varying the DC voltage applied to electrode 1.

The upper limit of DC voltage possible from the power amplifier that will be used in the experimental work later is 120 V, which, from (3), allows for the creation of spring constants up to -15.8 N/m, which result in the electrostatically-softened out-of-phase and in-phase mode frequencies shown in Tab. I. From (9) and (10), it has been found that the sensitivity of the amplitude ratio to a given stiffness perturbation is increased when the strength of the coupling spring is decreased. It is noted from (2) that weakening the coupling spring, k_c , will result in the convergence of the two mode frequencies. Therefore, the optimal value of k_c is the weakest value that maintains a separation of the mode frequencies, Δf , that avoids mode-aliasing. Previously reported research has shown that a Δf that is double the 3 dB bandwidth, Δf_{3dB} , of the resonant peaks is sufficient [19]. In addition, the fabricated devices have been tested under vacuum, which allowed for damping to be neglected in the theoretical model and results in a higher quality (Q) factor, which reduces Δf_{3dB} , minimizing mode-aliasing.

D. Actuation and sensing

The devices have been designed to be actuated by applying an AC voltage to electrode 1, which creates an electrostatic force on resonator 1 that alternates at the same frequency as the applied electrical signal.

The vibrating resonators create motional currents from the capacitive transduction gaps between each resonator and its neighboring fixed electrode. The frequency and amplitude of the vibrations of the two resonators are extracted by measuring motional current, using transimpedance amplifiers (TIAs) that are connected to resonator 1 and electrode 2. The design of the output circuitry, which is capable of converting alternating motional currents of the scale of nanoamperes to voltages up to 0.5 V, will be detailed in section V-B.

IV. FEM SIMULATIONS

The designs of the coupled MEMS resonator devices have simulated using the FEM simulation software *CoventorWare*. The resonant frequencies and the response of the amplitude ratios to a stiffness perturbation have been simulated and compared to theoretical predictions.

A. Model design

As with the SOI wafer that has been used to fabricate the actual devices, the FEM model has a Si layer of $50 \mu\text{m}$ with a Young's modulus, E , of 169 GPa and a density, ρ , of 2330 kg/m^3 . The fixed electrodes and the pair of resonators have been defined according to the schematic in Fig. 2, with three models created with three different anchor beam lengths of 55, 80 and $105 \mu\text{m}$.

The boundary conditions of the FEM model have been defined so that the anchors of the resonators are fixed, but allow for elastic energy loss ("anchor damping"), which will occur in a fabricated device. In addition, atmospheric damping has been included in the model with the air pressure surrounding the device being set to 0.1 mbar, achievable in the vacuum chamber that has been used for our experimental work.

The DC bias voltages have been set to be 0 V on resonator 1 and -120 V on resonator 2, creating an electrostatic spring of 15.8 N/m . Initially, electrode 1 and electrode 2 have been set to 120 V and 0 V, respectively, resulting in equal levels of electrostatic spring softening on each of the resonators, so that $k_1 = k_2 = k$. In preparation for FEM analysis, the model has been meshed into cubic elements of dimensions $5 \mu\text{m} \times 5 \mu\text{m} \times 5 \mu\text{m}$, which allowed for the fastest simulation time without sacrificing result accuracy.

B. Stiffness perturbation simulations

A modal simulation has been performed by applying an alternating force to resonator 1, replicating the electrostatic force that a 1 V peak-to-peak sinusoidal AC voltage would exert. The frequency of the force has been swept through a range, in order for the solver to determine the out-of-phase and in-phase mode frequencies. The simulated 3D mode-shape at the in-phase mode frequency is shown in Fig. 4.

For the model with $105 \mu\text{m}$ anchor beams, the out-of-phase and in-phase mode frequencies have simulated values of 402.450 kHz and 402.893 kHz, respectively, which are 4.3 % lower than the theoretical values in Tab. I, attributable to the inclusion of damping in the model. The amplitude ratio at both mode frequencies has been simulated to be 1:1, which is to be expected in a perfectly balanced system.

The simulation has been repeated with a stiffness perturbation, Δk , introduced to resonator 1, so that $k_1 = k + \Delta k$. The DC voltage of electrode 1 has been reduced from 120 V, which decreases the electrostatic spring softening in accordance with (13). The result of the perturbation is the increase of the effective stiffness, k_1 , of resonator 1, while maintaining the effective stiffness, k_2 , of resonator 2. Several simulations have been performed for increasing values of stiffness perturbation, with the simulated amplitude ratio being

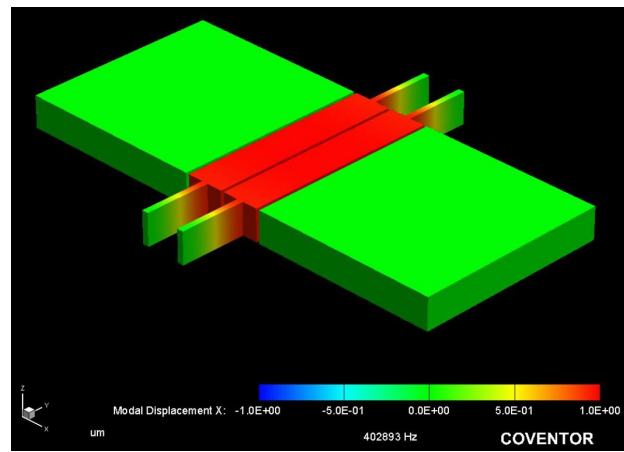


Fig. 4. 3D mode shape for the in-phase frequency of 402.893 kHz. Anchor beam length = $105 \mu\text{m}$. The maximum displacement is normalized to 1 (red) with the anchors and electrodes fixed with a displacement of 0 (green).

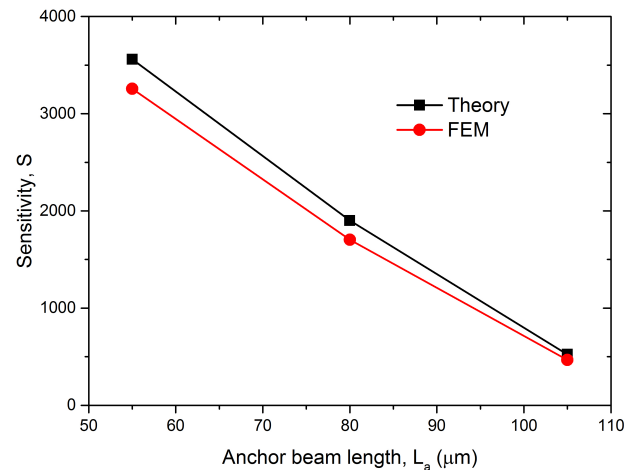


Fig. 5. FEM simulated and theoretical influence of anchor beam length on device sensitivity.

extracted each time. Furthermore, FEM simulations have been performed on the device models with $55 \mu\text{m}$ and $80 \mu\text{m}$ anchor beam lengths. The sensitivity for each of the three designs has been determined from the simulation results, and is shown in Fig. 5 as well as the theoretically predicted sensitivity, determined from the amplitude ratio response calculated from (10).

It can be seen from Fig. 5 that the FEM simulated amplitude ratio response shows good agreement with the theoretical predictions for all three device designs with the sensitivity of the device, as defined previously, increasing as a function of the anchor beam length, with shorter lengths resulting in more sensitive devices. From (10), it is noted that the initial balanced effective stiffness, k , of the resonators does not influence the amplitude ratio response to the perturbation Δk . Therefore, a device's sensitivity, defined by its response to the relative stiffness change, $\Delta k/k$, will be increased for a higher initial balanced effective stiffness k , which has been confirmed by the FEM simulations.

The theoretical and the simulated results in Fig. 5 show that

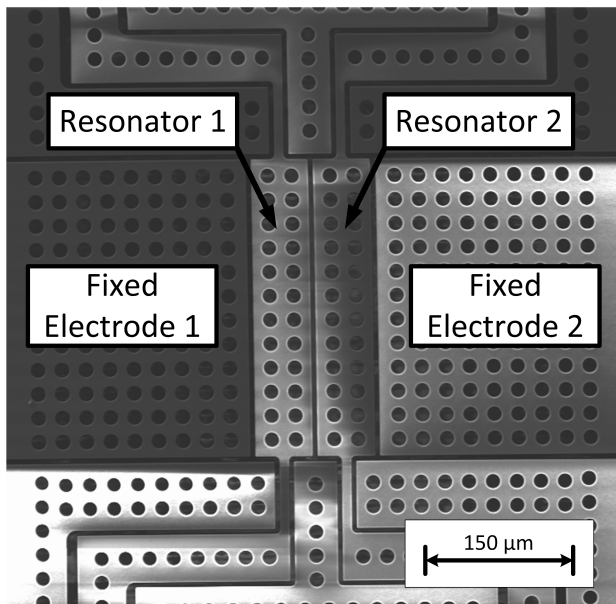


Fig. 6. SEM image of fabricated coupled resonator device with anchor beam length of 55 μm .

the simulated sensitivity remains within 9 % of the theoretically predicted value. The difference between the theory and the FEM simulated result is attributable to the variation of the coupling spring strength caused by the shift in the amplitude ratio, which is included in the FEM simulation but not the theoretical model that assumes a constant value.

V. EXPERIMENTAL PROCEDURE

A. MEMS fabrication

The three different devices with anchor beam lengths of 55 μm , 80 μm and 105 μm have been fabricated using the SOI process that has been described in section III. A scanning electron micrograph (SEM) of a fabricated device with 55 μm anchor beams is shown in Fig. 6. The image shows the release holes, which allowed for the removal of a block of the handle wafer below the MEMS structure. The coupling gaps between the resonators and between each resonator and its neighboring electrode have been designed to be 5 μm and visual inspection of the fabricated devices showed that the trenches had a width of $5 \pm 0.1 \mu\text{m}$.

The devices have been designed with bonding pads of minimum dimensions 300 $\mu\text{m} \times 300 \mu\text{m}$, which is large enough to allow for wire bonds to be accurately secured to the pad. The chip containing the devices has been secured in a chip carrier and wire-bonded, to allow for the necessary input and output connections to be made to the device. A further advantage of the fabrication process used for this work is that it does not require a metallization step, so the bonding can be made directly to the silicon device layer. The resistivity of the device layer is between 0.001 Ωcm and 0.003 Ωcm , which is low enough to allow for an ohmic connection to be made to the bonding wire.

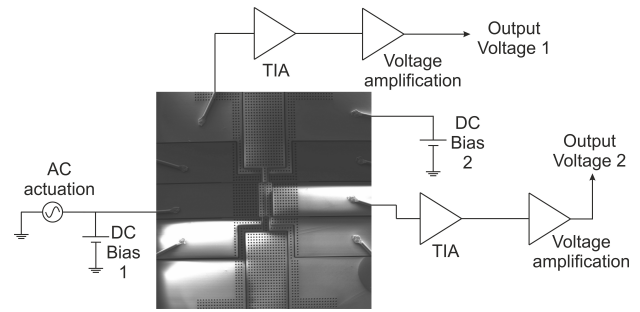


Fig. 7. Experimental set-up. MEMS device has been wire-bonded to carrier positioned on printed circuit board containing output circuitry.

B. Measurement set-up

The wire-bonded MEMS chip has been plugged into a socket that has been mounted on a printed circuit board (PCB) that contains the necessary input and output circuitry. Fig. 7 shows an SEM of a bonded MEMS device and the connections to the schematic of the PCB circuitry.

As explained previously (section III), electrostatic spring softening has been introduced to the two resonators by applying a positive DC voltage to electrode 1 (DC bias 1) and a negative DC voltage to resonator 2 (DC bias 2). Both resonator 1 and electrode 2 are held at 0 V, as they are connected to the inputs of two TIAs. If the two DC bias voltages are of an equal magnitude but opposite polarity, then an equal value of electrostatic spring softening will be applied to each resonator, in accordance with (13). In addition, the electrostatic coupling spring between the two resonators has been created from the potential difference, ΔV , between the negative DC voltage on resonator 2 and 0 V on resonator 1.

For this work, DC bias 1 has been set at 120 V and DC bias 2 has been set at -120 V, resulting in a coupling spring, k_c , of -15.8 N/m and electrostatic spring softening, k_{elec} , of -15.8 N/m on both resonators. Using a coupling spring of -15.8 N/m should result in the out-of-phase and in-phase frequencies shown in Tab. I, ensuring sufficient ($2 \times \Delta f_{3dB}$) separation of the two resonant peaks, minimizing mode-aliasing. The resonators have been driven by applying an AC sinusoidal voltage from a signal generator to electrode 1. A 1 V peak-to-peak signal has been used as this has been found to drive the resonators with negligible non-linear behavior, so the peaks can be reliably measured.

The vibration amplitude ratio of the coupled resonator pair has been extracted by measuring the motional currents from the capacitive transduction gaps between each resonator and its neighboring electrode. The motional currents, i , are determined by the velocity, \dot{x} , of the resonators, from the expression $i = \eta \dot{x}$, where η is the transduction factor. The amplitude ratio of the alternating motional current signals is equivalent to the vibration amplitude ratio of the resonators. As can be seen from Fig. 7, the motional currents from the vibrating resonators have been converted to voltage signals, using two TIAs (OPA657 from Texas Instruments). Subsequently, the voltage signals from the TIAs have been amplified (AD8065 from Analog Devices) to give output voltages of at least 100 mV amplitude. A noise floor of 20 μV has been measured

TABLE II
EXPERIMENTALLY MEASURED MODE FREQUENCIES AND
CORRESPONDING CALCULATED EFFECTIVE STIFFNESS

Anchor beam length (μm)	Measured modes		
	f_{op} (kHz)	f_{ip} (kHz)	$k_{1,2}$ (N/m)
55	1041.223	1041.605	95232
80	757.381	758.184	50863
105	328.005	328.543	9292

for the output voltage signals.

A spectrum analyzer (Rohde and Schwarz FSV 3) has been used to measure the output voltage signal from resonator 1 and resonator 2. The AC input signal has been swept across a frequency range while the amplitude of the output voltages is being measured. The out-of-phase and in-phase mode frequencies have been identified as the frequencies with the largest amplitudes. After identifying the modes, the frequency sweep range of the actuation signal is narrowed and the peak frequency and amplitude are measured for the in-phase mode for both resonator 1 and resonator 2. By comparing the amplitudes of the output voltage signals at the in-phase mode frequency, the vibration amplitude ratio of the resonator pair can be extracted.

The characterization experiments have been performed with the PCB secured in a vacuum chamber. The pressure inside the chamber has been maintained at 3×10^{-5} mbar, minimizing atmospheric damping and allowing for high-Q resonant peaks to be achieved. The temperature of the chamber has not been controlled, so the experiments have been conducted at room temperature. The necessary electrical connections to the PCB have been made possible through use of feedthroughs, allowing DC and AC voltages to be applied and the output signals to be measured.

VI. MEASUREMENT RESULTS AND DISCUSSION

A. Frequency response

The previously outlined measurement method has been used to extract the out-of-phase and in-phase mode frequencies of each of the three device designs (55 μm , 80 μm and 105 μm anchor beam length). The measured values are shown in Tab. II. The variation between the measured values and the theoretical values in Tab. I is likely as a result of fabrication tolerances and intrinsic stress in the SOI device layer. Taking the measured values for the mode frequencies, an estimation of the actual effective stiffness, k_1 and k_2 , for each of the three resonator designs at the initial balanced state has been calculated using (5), with the values shown in Tab. II.

As explained previously, starting from a balanced state, the two mode frequencies should diverge in response to a stiffness imbalance between the resonators. Fig. 8 shows the the experimentally measured difference between the out-of-phase and in-phase mode frequencies, for a device with 105 μm anchor beams, in response to an electrostatically induced stiffness increase on resonator 1. It can be seen that the frequency difference increases as a function of the stiffness perturbation, as expected. An initial imbalance would be expected between

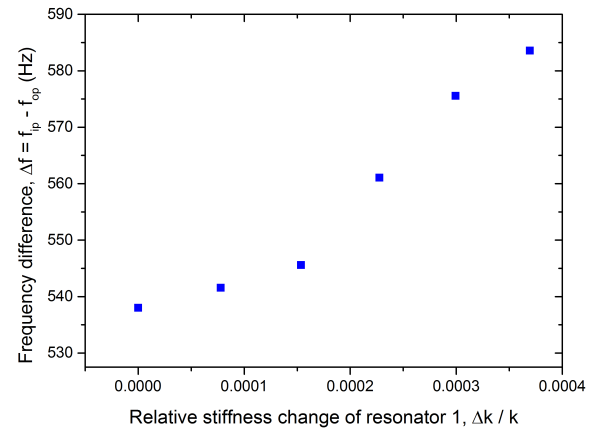


Fig. 8. Measured response of frequency difference between the out-of-phase and in-phase modes for 2-DOF system to a relative stiffness change on resonator 1. The device measured has anchor beams with a length of 105 μm .

TABLE III
EXPERIMENTALLY MEASURED DEVICE CHARACTERISTICS

Anchor beam length (μm)	Q-factor	3 dB bandwidth, Δf_{3dB} (Hz)	Mode separation, Δf (Hz)
55	11768	88	538
80	6535	116	685
105	1950	169	382

the resonators, due to fabrication tolerances and the trend shown in Fig. 8 suggests that for this device, resonator 1 has a stiffness that is about 0.02 % lower than resonator 2. Similar initial stiffness imbalances have been measured for all the devices in this work, so the previously calculated and simulated linear responses of the amplitude ratio to a stiffness perturbation (Fig. 5) are expected to be valid.

The Q-factor of the modes for each device have been measured and are shown in Tab. III, along with the 3 dB bandwidth, Δf_{3dB} , of the peaks. It can be seen that the separation of the out-of-phase and in-phase mode frequencies, Δf , is at least $2 \times \Delta f_{3dB}$, so mode-aliasing does not occur [19].

For the device with 105 μm anchor beams, for a relative stiffness increase of 0.0004 for resonator 1, the in-phase mode frequency increased by 53 Hz, representing a relative increase of 0.016 %. Using the definition of (6), the frequency sensitivity has been calculated to be 0.4, which will be compared to the sensitivity of the amplitude ratio shift in the following section.

B. Mode localization response to stiffness perturbation

The experimentally measured amplitude ratio change, $\Delta(x_1/x_2)$, in response to an electrostatically induced relative stiffness increase, $\Delta k/k$, on resonator 1 is shown in Fig. 9, for all three device designs, along with the FEM simulated response.

The graph of Fig. 9 shows the expected trend of increasing amplitude ratio, x_1/x_2 , as a function of increasing stiffness imbalance in the resonator pair. It can be seen that the measured values show good agreement with the simulated

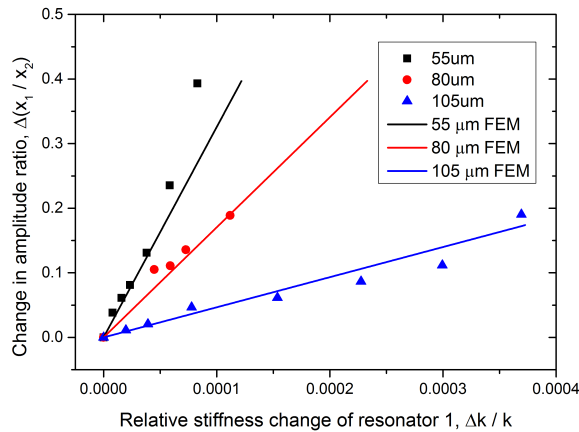


Fig. 9. Measured response of amplitude ratio of 2-DOF system to a relative stiffness change on resonator 1 for devices with 55 μm , 80 μm and 105 μm anchor beam lengths.

TABLE IV
EXPERIMENTALLY DERIVED DEVICE SENSITIVITIES

Anchor beam length (μm)	Sensitivity	Sensitivity normalized to f_0
55	3257	3.13
80	1704	2.25
105	466	1.42

values, confirming the validity of both the theoretical equation (10) and the FEM model.

From (10), it is noted that the initial effective stiffness does not feature, with the coupling spring constant, k_c , and the change in stiffness of resonator 1, Δk , determining the amplitude ratio of the resonators at the in-phase mode frequency. Therefore, it is expected that a higher initial effective stiffness, k , leads to higher sensitivity with respect to relative stiffness change, $\Delta k/k$, as has been confirmed from the experimental measurements (Fig. 9).

C. Device sensitivity and discussion

From the amplitude ratio responses shown in Fig. 9, the sensitivities of the different device designs have been calculated and are listed in Tab. IV. It can be seen that the sensitivity for the coupled resonator devices increases when the length of the anchor beam, L_a , is decreased. Even if the sensitivity values are normalized to the resonant frequency, an increase in sensitivity is seen.

Taking the measurements from the device with 105 μm anchors, it was demonstrated that the amplitude ratio shift, $\Delta(x_1/x_2)$, of a coupled resonator system is more sensitive to a stiffness imbalance, $\Delta k/k$, than the relative in-phase mode frequency shift, $\Delta f/f$, (equivalent to resonant frequency shift of a 1-DOF system), with a four orders of magnitude difference, comparing a sensitivity of 0.4 for relative frequency shift to a sensitivity of 466 for amplitude ratio shift. Similarly, for the device with 55 μm anchor beams, the sensitivity of the in-phase resonant frequency to a relative stiffness change is 0.134, whereas the sensitivity of the amplitude ratio is 3257, also representing a four orders of magnitude increase. The

findings agree with previously published studies [17], which characterized coupled resonators of the double-ended tuning fork design.

The best example of stiffness sensing for a 2-DOF coupled resonator system in literature [17] shows a sensitivity of 356, if the sensitivity definition in (11) is applied. From Tab. IV, it can be seen that the best sensitivity demonstrated in this work, 3257, is 9 times greater than the state of the art, demonstrating the importance of dimension variation in the design of 2-DOF coupled resonator sensors.

In this work, the signal-to-noise ratio (SNR) for each of the output voltage signals from the resonators has been measured as 7.87 dB for a relative stiffness change, $\Delta k/k$, of 0.8×10^{-6} . The noise for the output signal of each resonator has been determined by measuring the variation in the amplitude of each output signal while the system is being driven at the in-phase mode. It has been found that reliably measuring a relative stiffness change smaller than 0.8×10^{-6} is not possible, as the noise in the output signals becomes comparable to the shift in amplitude induced by the stiffness change.

In addition to the improved sensitivity that has been demonstrated by the device design characterized in this work, the design has a larger surface area, which can prove advantageous for mass sensing. For example, the surface can be biologically functionalized so that an antigen of interest will bind to one of the resonators causing an imbalance. A further advantage of the device design is that the SOI fabrication process has been shown to have a high yield of over 95 % [24], which has been confirmed during the wafer-level fabrication for this work.

VII. CONCLUSION

This paper has characterized the mode-localization behavior of 2-DOF electrostatically-coupled MEMS resonator devices, that have been fabricated using a high-yield, dicing-free SOI process. The devices have a novel design architecture, when compared to previously reported work. The length of the anchor beams of the resonators has been varied between three different device designs, with a shorter length resulting in higher resonant mode frequencies for the coupled system. In addition, it has been determined that the sensitivity of the amplitude ratio of the coupled system to an electrostatically-induced stiffness imbalance is higher for a shorter anchor beam length, with a sensitivity that is four orders of magnitude greater than the frequency sensitivity of a 1-DOF system, and is 9 times greater than the best previously reported 2-DOF system.

In addition, the devices in this work have been designed to facilitate mass sensing and their sensitivity to stiffness imbalance demonstrates that they have the potential to be utilized in a mass sensing capacity.

REFERENCES

- [1] M. Ahmed, D. Butler, and Z. C. Butler, "MEMS Relative Pressure Sensor on Flexible Substrate," in *Proc. IEEE Sensors Conf.*, Oct. 2011, pp. 460-463.
- [2] A. L. Roy, H. Sarker, A. Dutta, and T. K. Bhattacharyya, "A high-precision SOI MEMS-CMOS +/- 4g piezoresistive accelerometer," *Sens. Actuators A, Phys.*, vol. 210, pp. 77-85, Apr. 2014.

- [3] T. Zawada, K. Hansen, R. Lou-Moeller, E. Ringgaard, T. Pedersen, and E. V. Thomsen, "High performance piezoelectric thick film based energy harvesting micro-generators for MEMS," in *Proc. Eurosensors XXIV*, Sep. 2010, pp. 1164-1167.
- [4] C. T.-C. Nguyen, "MEMS Technology for Timing and Frequency Control," *IEEE Trans. Ultrason., Ferroelectr. Freq. Control*, vol. 54, no. 2, pp. 251-270, Feb. 2007.
- [5] A.-C. Wong and C. T.-C. Nguyen, "Micromechanical Mixer-Filters ("Mixlers")," *J. Microelectromech. Syst.*, vol. 13, no. 1, pp. 100-112, Feb. 2004.
- [6] K. E. Wojciechowski, B. E. Boser, and A. P. Pisano, "A MEMS Resonant Strain Sensor Operated in Air," in *Proc. 17th IEEE Int. Conf. Microelectromech. Syst.*, Jan. 2004, pp. 841-845.
- [7] R. G. Azevedo, D. G. Jones, A. V. Jog, B. Jamshidi, D. R. Myers, L. Chen, X.-A. Fu, M. Mehregany, M. B. J. Wijesundara, and A. P. Pisano, "A SiC MEMS Resonant Strain Sensor for Harsh Environment Applications," *IEEE Sensors J.*, vol. 7, no. 3-4, pp. 568-576, Apr. 2007.
- [8] R. Melik, E. Unal, N. K. Perkgoz, C. Puttlitz, and H. V. Demir, "Circular High-Q Resonating Isotropic Strain Sensors with Large Shift of Resonance Frequency under Stress," *Sensors*, vol. 9, no. 12, pp. 9444-9451, Dec. 2009.
- [9] A. A. Seshia, M. Palaniapan, T. A. Roessig, R. T. Howe, R. W. Gooch, T. R. Schimert, and S. Montague, "A Vacuum Packaged Surface Micromachined Resonant Accelerometer," *J. Microelectromech. Syst.*, vol. 11, no. 6, pp. 784-793, Dec. 2002.
- [10] A. Somà and A. Ballestra, "Residual stress measurement method in MEMS microbeams using frequency shift data," *J. Micromech. Microeng.*, vol. 19, no. 9, Sep. 2009.
- [11] H. Zhang and E. S. Kim, "Micromachined Acoustic Resonant Mass Sensor," *J. Microelectromech. Syst.*, vol. 14, pp. 699-706, Aug. 2005.
- [12] K. L. Ekinici, X. M. H. Huang, and M. L. Roukes, "Ultrasensitive nanoelectromechanical mass detection," *Appl. Phys. Lett.*, vol. 84, no. 22, pp. 4469-4471, May 2004.
- [13] S. B. Patil, V. Chu, and J. P. Conde, "Mass Sensing using an Amorphous Silicon MEMS resonator," in *Proc. Eurosensors XXIII*, Sep. 2009, pp. 1063-1066.
- [14] K. Y. Gfeller, N. Nugaeva, and M. Hegner, "Micromechanical oscillators as rapid biosensor for the detection of active growth of *Escherichia coli*," *Biosensors and Bioelectron.*, vol. 21, no. 3, Sep. 2005.
- [15] A. P. Davila, J. Jang, A. K. Gupta, T. Walter, A. Aronson, and R. Bashir, "Microresonator mass sensors for detection of *Bacillus anthracis* Sterne spores in air and water," *Biosensors and Bioelectron.*, vol. 22, no. 12, Jun. 2007.
- [16] P. W. Anderson, "Absence of Diffusion in Certain Random Lattices," *Phys. Rev.*, vol. 109, no. 5, pp. 1492-1505, Mar. 1958.
- [17] P. Thiruvengatanathan, J. Yan, J. Woodhouse, and A. A. Seshia, "Enhancing Parametric Sensitivity in Electrically Coupled MEMS Resonators" *J. Microelectromech. Syst.*, vol. 18, no. 5, pp. 1077-1086, Oct. 2009.
- [18] M. Manav, G. Reynen, M. Sharma, E. Cretu, and A. S. Phani, "Ultrasensitive resonant MEMS transducers with tuneable coupling," *J. Micromech. Microeng.*, vol. 24, no. 5, May 2014.
- [19] C. Zhao, G. S. Wood, J. Xie, H. Chang, S. H. Pu, and M. Kraft, "A force sensor based on three weakly coupled resonators with ultrahigh sensitivity," *Sens. Actuators A, Phys.*, vol. 232, Aug. 2015, pp. 151-162.
- [20] P. Thiruvengatanathan, J. Yan, J. Woodhouse, A. Aziz, and A. A. Seshia, "Ultrasensitive mode-localized mass sensor with electrically tunable parametric sensitivity," *Appl. Phys. Lett.*, vol. 96, no. 8, Feb. 2010.
- [21] M. Spletzer, A. Raman, A. Q. Wu, X. Xu, and R. Reifengerger, "Ultrasensitive mass sensing using mode localization in coupled microcantilevers," *Appl. Phys. Lett.*, vol. 88, no. 25, Jun. 2006.
- [22] M. Spletzer, A. Raman, H. Sumali, and J. P. Sullivan, "Highly sensitive mass detection and identification using vibration localization in coupled microcantilever arrays," *Appl. Phys. Lett.*, vol. 92, no. 11, Mar. 2008.
- [23] G. S. Wood, C. Zhao, S. H. Pu, I. Sari, and M. Kraft, "Sensor Based on the Mode-Localization Effect in Electrostatically-Coupled MEMS Resonators Fabricated Using an SOI Process," in *Proc. IEEE Sensors Conf.*, Nov. 2015.
- [24] I. Sari, I. Zeimpekis, and M. Kraft, "A dicing free SOI process for MEMS devices," *Microelectron. Eng.*, vol. 95, pp. 121-129, Jul. 2012.
- [25] P. Thiruvengatanathan, J. Woodhouse, J. Yan, and A. A. Seshia, "Manipulating Vibration Energy Confinement in Electrically Coupled Microelectromechanical Resonator Arrays" *J. Microelectromech. Syst.*, vol. 20, no. 1, pp. 157-164, Feb. 2011.
- [26] F. J. Giessibl, "A direct method to calculate tip-sample forces from frequency shifts in frequency-modulation atomic force microscopy" *Appl. Phys. Lett.*, vol. 78, no. 1, pp. 123-125, Jan. 2001.



Graham S. Wood (M'10) received the M.Eng degree in electronics and electrical engineering and the M.Sc by Research degree in microelectronics from the University of Edinburgh, Edinburgh, U.K., in 2008 and 2011, respectively, and the Ph.D degree in microelectromechanical systems from the University of Southampton, Southampton, U.K., in 2016.

He is currently a Research Associate with the Scottish Microelectronics Centre, Institute for Integrated Micro and Nano Systems, School of Engineering, University of Edinburgh. From June 2008 until April 2010, he held the same position, where he conducted research concerning the actuation and sensing of SiC MEMS resonators for high-frequency RF applications. His current research involves the use of graphene resonating structures as acoustic transducers.



Chun Zhao (S'14-M'16) received the B.Eng. degree in measurement & control technology and instrument from the Huazhong University of Science and Technology, Wuhan, China, in 2009, the M.Sc. degree in analog and digital IC design from Imperial College London, London, U.K., in 2011, and the Ph.D degree in microelectromechanical systems from the University of Southampton, Southampton, U.K., in 2016.

He is currently a Research Associate in MEMS with the Nanoscience Centre, Department of Engineering, University of Cambridge. From April 2015 to March 2016, he was a Research Scientist with Sharp Laboratories of Europe, Oxford, U.K, working on the research and development of acoustic MEMS devices and control circuit design. His current research interests include micro-electromechanical systems (MEMS), miniature sensing devices, micro-resonators and interface circuit for sensors design.



Suan Hui Pu (S'09-M'11) received the M.Eng. degree in mechanical engineering from Imperial College London, London, U.K. in 2006 and the Ph.D. degree in electrical and electronic engineering from Imperial College London, London, U.K. in 2010.

He was a Product Engineer with Infineon Technologies (Kulim) Sdn. Bhd., from 2010 to 2012, working on yield enhancement for a bipolar-CMOS-DMOS process technology. He is currently an Assistant Professor at the University of Southampton Malaysia Campus and a visiting academic in the Nano Research Group, School of Electronics and Computer Science, University of Southampton, U.K. He has published more than 16 peer-reviewed papers in international journals and conferences. His current research interests include MEMS/NEMS sensors and actuators, graphene, nanocrystalline graphite and wearable technology.

Dr. Pu is currently serving as a technical committee member for IEEE Electronics Packaging Technology Conference (EPTC). He is a reviewer for IEEE Journal of Microelectromechanical Systems and IEEE Transactions on Components, Packaging and Manufacturing Technology.



Ibrahim Sari received the B.Sc degree in mechanical engineering, the M.Sc degree in control systems theory and applications and the Ph.D degree in microelectromechanical systems (MEMS) based vibration energy harvesting from Middle East Technical University, Ankara, Turkey, in 1999, 2002, and 2008, respectively.

He was a Research Fellow with the Nano Research Group, School of Electronics and Computer Science, University of Southampton, Southampton, U.K., from 2008 to 2012, where he investigated

novel techniques on levitation and propulsion of micro-objects using electromagnetic fields. In parallel to this role, he has developed novel MEMS fabrication techniques focusing on dicing free release and fabrication methods that can be used for the production of SOI-MEMS (Silicon-on-Insulator MEMS) inertial sensors. The techniques he has developed has been used in several academic and commercial projects to fabricate high-performance MEMS actuators and sensors. He is currently the Commercial Processing Manager at the Southampton Nanofabrication Centre, Southampton, U.K., where he is managing and organizing the nano- and micro-fabrication focused commercial business activities.



Michael Kraft received a Dipl.-Ing. degree in electrical and electronics engineering from the Friedrich-Alexander University at Erlangen-Nürnberg, Germany, in 1993, and a Ph.D. degree from Coventry University, U.K., in 1997.

From 1998 to 1999, he was with the Berkeley Sensors and Actuator Center, University of California, Berkeley, USA, working on integrated microelectromechanical systems (MEMS) gyroscopes. He was a faculty member of the School of Electronics and Computer Science, University of Southampton,

U.K., from 1999 to 2012, where he also acted as the Director of the Southampton Nanofabrication Centre from 2010 to 2012. He then joined the Fraunhofer Institute for Microelectronic Circuits and Systems, Duisburg, Germany, from 2012 to 2014, where he was the Head of the Department of Micro- and Nanosystems with a focus on fully integrated microsensors and biohybrid systems. Concurrently, he held the Professorial Chair (W3) of Integrated Micro- and Nanosystems at the University of Duisburg-Essen. He is currently a Professor of Micro- and Nanosystems at the University of Liège, Belgium. He has authored or co-authored over 200 peer-reviewed journal and conference papers. He has contributed to three textbooks on MEMS and edited a book on MEMS for Aerospace and Automotive Applications. His research interests include MEMS and nanotechnology ranging from process development to system integration of MEMS and nanodevices.

Dr. Kraft has served on several steering and technical committees of international conferences, such as the IEEE Sensors, Eurosensors, and the Micromechanics and Microsystems Europe Workshop.